

Pair-density-wave superconductivity: a microscopic model on 2D honeycomb lattice

Yi-Fan Jiang^{1,*} and Hong Yao^{2,†}

¹*School of Physical Science and Technology, ShanghaiTech University, Shanghai 201210, China*

²*Institute for Advanced Study, Tsinghua University, Beijing 100084, China*

(Dated: October 29, 2024)

Pair-density-wave (PDW) is a long-sought exotic state with oscillating superconducting order without external magnetic field. So far it has been rare in establishing a 2D microscopic model with PDW long-range order in its ground state. Here we propose to study PDW superconductivity in a minimal model of spinless fermions on the honeycomb lattice with nearest-neighbor (NN) and next-nearest-neighbor (NNN) interaction V_1 and V_2 , respectively. By performing a state-of-the-art density-matrix renormalization group (DMRG) study of this t - V_1 - V_2 model at finite doping on six-leg and eight-leg honeycomb cylinders, we showed that the ground state exhibits PDW ordering (namely quasi-long-range order with a divergent PDW susceptibility). Remarkably this PDW state persists on the wider cylinder with 2D-like Fermi surfaces (FS). To the best of our knowledge, this is probably the first controlled numerical evidence of PDW in systems with 2D-like FS.

In conventional BCS theory, two electrons pair with zero center-of-mass momentum and pairing amplitude respects translational symmetry [1]. Nonetheless, it was proposed later by Fulde-Ferrell-Larkin-Ovchinnikov (FFLO) that superconducting states with finite-momentum pairing can occur in weakly interacting systems with external magnetic field [2, 3]. Although evidences of the FFLO state has been reported in a few quantum materials [4–11], it remains elusive to unambiguously establish FFLO states experimentally.

Recently pair-density-wave (PDW) was introduced as an exotic superconducting state with finite-momentum pairing (namely its pairing amplitude oscillates in real space), without the need of applying external magnetic field [12]. Increasing interest has been focused on evidences of PDW in quantum materials such as underdoped cuprate superconductors [13–22], iron-based superconductors [23, 24], heavy-fermion materials [25, 26], and kagome superconductors [27]. These novel PDW states have spatial pairing modulation similar to the FFLO state, but appear without external magnetic field. It is widely believed that PDW in those systems emerges mainly due to strong correlations. Nonetheless, it remains a challenge to obtain controlled or reliable evidences of PDW in two and higher dimensional microscopic models, despite mean field and other studies have shown that PDW states may be realized in ground states of microscopic models [28–58].

So far, controlled numerical evidence of PDW has been shown in density-matrix renormalization group (DMRG) studies of quasi-1D models, including Refs. [59–65]. (Note that DMRG studies of doped candidate quantum spin liquid models have observed quasi-long-range PDW correlation with finite PDW susceptibility [66–68].) More recently, DMRG evidence of PDW is observed in the strong coupling limit of the Holstein-Hubbard model with a single 1D-band crossing on Fermi surface (FS) [69]. Evidence of PDW in 2D models with 2D-like FS has not been established yet in controlled DMRG calculations.

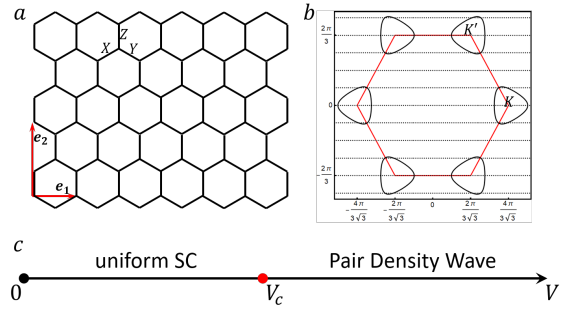


FIG. 1. (a) The example of honeycomb lattice with $N = 2 \times 6 \times 6$. The boundary condition is open along \hat{e}_1 direction but periodic along \hat{e}_2 . X , Y and Z define three types of bonds. (b) The Fermi surface of the doped spinless model: it has two hole pockets around the K and K' points. Dash lines are the eight cuts with different k_y momentum for eight-leg cylinder. (c) The quantum phase diagram of the spinless t - V_1 - V_2 model with light doping δ , as a function of interaction strength V . Here we mainly focus on $\delta = 1/9$, $V_1 = -V$, and $V_2 = V/2$. Our study further demonstrates that the PDW phase can emerge in a finite range of V_2/V_1 ratios and doping levels (see the SM for more details).

Here we employ DMRG [70] to explore possible evidences of PDW in a 2D fermion model on honeycomb lattice with attractive nearest-neighbor (NN) V_1 and repulsive next-nearest-neighbor (NNN) interaction V_2 away from half filling. It was previously suggested in Ref. [40] that, at half filling, PDW with intra-valley pairing can emerge in the ground state of the t - V_1 - V_2 model; moreover the PDW transition features emergent supersymmetry. It was argued that, *at half filling*, PDW wins over uniform pairing because PDW can fully gap out the Dirac cones but uniform BCS pairing cannot. Nonetheless, it remains elusive if at half filling PDW emerges from exact-diagonalization study of the half-filling model on a small cluster [71, 72]. So, it is natural to ask whether PDW occurs in the t - V_1 - V_2 model from large-scale calculations on systems with much larger size approaching 2D.

From state-of-the-art DMRG study of the t - V_1 - V_2 model *away from half filling*, we shows reliable evidences of PDW in the doped model with two hole pocket Fermi surfaces around the two Dirac points $\pm K$. Specifically, we find pairing between two electrons on the same hole pocket (namely intra-valley pairing) emerges in the ground state, leading to a PDW state. Our DMRG calculations, greatly enhanced by GPU accelerations, enable us to simulate the model on the eight-leg cylinders featuring 2D-like FS for the first time; our simulations on the wider cylinders remarkably revealed that the PDW state persists in the model with a 2D-like FS, which is beyond 1D systems. To the best of our knowledge, this is probably the first controlled numerical evidence substantiating the existence of PDW in systems exhibiting a 2D-like FS. Moreover, a 2D t - V_1 - V_2 spinless fermion model hosting a PDW ground state may be potentially realized in various spin-polarized electron systems such as twisted moire systems [73–77], ultracold fermions [78, 79], and Fe-based compounds with strong Hund’s coupling [80].

Model: We now consider the spinless fermion model on honeycomb lattice with density-density interactions described by the following Hamiltonian

$$H = -t \sum_{\langle ij \rangle} (c_i^\dagger c_j + h.c.) + V_1 \sum_{\langle ij \rangle} n_i n_j + V_2 \sum_{\langle\langle ij \rangle\rangle} n_i n_j, \quad (1)$$

where c_i^\dagger is the electron creation operator on site $i = (x_i, y_i)$ and $n_i = c_i^\dagger c_i$ is electron number operators. Here t denotes NN hopping amplitude and we set $t = 1$ as the energy unit. The strength of the NN density-density interaction is labeled by V_1 and the NNN interaction V_2 . We focus on the case of $V_1 = -V$ and $V_2 = \frac{V}{2}$, and look for possible PDW ordering by varying V . The PDW order in the models with other V_2/V_1 ratios and different doping concentrations is also studied, as detailed in Supplemental Materials (SM).

We employ DMRG to study the t - V_1 - V_2 model on honeycomb lattice with cylindrical geometry, as depicted in Fig. 1(a), where we take the periodic boundary condition in the $\mathbf{e}_2 = (0, \frac{3}{2})$ direction and open boundary condition in the $\mathbf{e}_1 = (\sqrt{3}, 0)$ direction. Here, we focus on cylinders with width L_y and length L_x , where L_y and L_x are number of unit cells along the armchair chain in the \mathbf{e}_2 and zigzag chain in the \mathbf{e}_1 directions, respectively. There are $N_c = L_x L_y$ number of unit cells (and $N = 2L_x L_y$ number of lattice sites). Suppose N_e denotes the number of electrons; at half filling, $N_e = N_c$ which is $N/2$. The concentration of doped holes is defined as $\delta = \frac{N_h}{N_c}$ with $N_h = N_c - N_e$. In the present study, we focus on $L_y = 6$ and $L_y = 8$ cylinders with L_x up to 48 at hole doping concentration $\delta \leq 1/8$. We perform up to 100 sweeps and keep up to 33,000 U(1) DMRG block states to obtain a typical truncation error $\epsilon \lesssim 5 \times 10^{-6}$. Further details of the numerical simulations are provided in the SM.

Quantum phase diagram: At doping slightly

away from half filling, the Fermi surface of the model in 2D becomes two hole pockets around two Dirac points $\pm K$ as shown in Fig. 1(b). In the non-interacting limit ($V = 0$), the single-particle dispersion is denoted as $\epsilon(\vec{k}) = -2t(\cos k_x + \cos k_y) - \mu$, where μ denotes the chemical potential; the susceptibility of uniform SC diverges logarithmically with temperature due to the nesting of the Fermi surface in the *particle-particle* channel, namely $\epsilon(\vec{k}) = \epsilon(-\vec{k})$, guaranteed by the inversion or time-reversal symmetry of the model. Consequently, when the interaction V is finite but sufficiently weak, uniform SC with usual zero-momentum pairing is expected in the ground state. Here, we are more interested in the regime beyond the weak coupling physics. Indeed, when V exceeds a critical value, our DMRG simulations show that the pair-pair correlation function starts to exhibit intense sign-changing oscillation at long distance, i.e. forming a PDW state. Correspondingly, the Fourier transformation of the scaled pair-pair correlation function exhibits two sharp peaks at non-zero momentum $Q \sim \pm 2K$, which implies that Cooper pairs in the PDW state consist of fermions from the same hole pocket. Interestingly, this PDW phase can be solely induced by V_1 and extends to a range of doping level around 10%. We would like to emphasize that the PDW here is incommensurate away half filling, importantly distinct from the possible commensurate PDW realized at half filling.

Here we would like to emphasize the key importance of 8-leg cylinder. As the cylinders respects translation symmetry along y , $k_y = 2\pi \frac{n_y}{L_y}$ with integer $n_y \in (-\frac{L_y}{2}, \frac{L_y}{2}]$ is a good quantum number; k_y can be employed to label bands and the total number of k_y bands is L_y . As width increases, the small Fermi pockets could be crossed by k_y bands with both $k_y = 0$ and non-zero k_y such that the system starts to approach to the 2D limit when more and more k_y bands cross the Fermi level. This condition is satisfied on the 8-leg systems which is studied in the present work. As a consequence, we start to observe the 2D-like behavior in such system, e.g. the density profile shows a tendency to restore the C_6 rotation symmetry of the 2D lattice on the eight-leg cylinders although the 8-leg cylinder still slightly breaks the C_6 symmetry. Remarkably, our DMRG study shows that the spatial oscillation of the pair-pair correlation function is still robust on 8-leg cylinders with moderate interaction and there are the pronounced peaks around $\pm 2K$ points. These numerical evidences indicate that the PDW ordering could persist in the minimal model Eq. (1) even when it starts to approach 2D with 2D-like FS. The quantum phase diagram of the doped 2D spinless model obtained from our DMRG study is sketched in Fig. 1(c).

PDW on six-leg cylinders: Possible SC ordering in the t - V_1 - V_2 model in Eq. (1) can be characterized by equal-time pair-pair correlations defined as

$$\Phi_{\alpha\beta}(r) = \left\langle \hat{\Delta}_\alpha^\dagger(x_0, y_0) \hat{\Delta}_\beta(x_0 + r, y_0) \right\rangle, \quad (2)$$

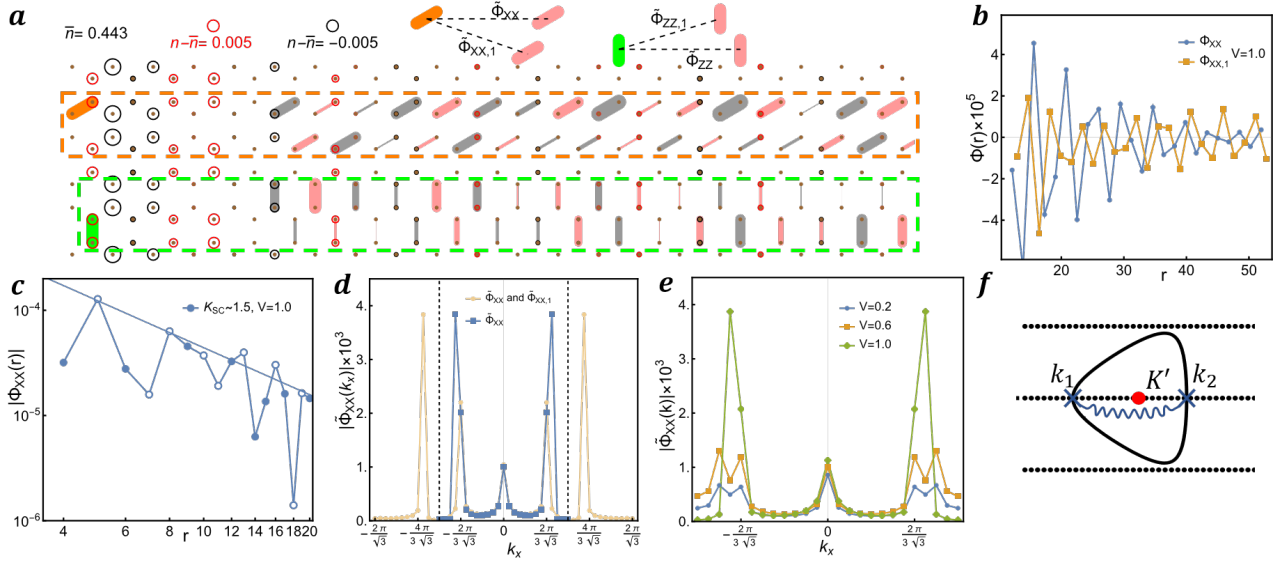


FIG. 2. DMRG results of PDW on the 6-leg cylinder: (a) Charge density profile and scaled pair-pair correlation functions $\tilde{\Phi}(r)$ of $V = 1.0$ model on $2 \times 48 \times 6$ cylinder with doping concentration $\delta \sim 11.1\%$. Radius of circles show the difference $n(x, y) - \bar{n}$ where \bar{n} is the average density, and thickness of bonds represent the amplitude of four types of $\Phi(r)$ illustrated on the top of figure. Negative values are marked black. (b) Pair-pair correlation function $\Phi_{XX}(r)$ and $\Phi_{XX,1}(r)$ of the same model. (c) Long-range behavior of $\Phi_{XX}(r)$ fitted by the power-law function $\sim r^{-K_{sc}}$, empty circles denote negative values. (d) Fourier transform of scaled correlation functions: Orange line presents the results based on $\tilde{\Phi}_{XX}(r)$ and $\tilde{\Phi}_{XX,1}(r)$ and blue line shows the results obtained from $\tilde{\Phi}_{XX}(r)$ alone. Dashed lines illustrate the folded Brillouin zone. (e) Fourier transform of scaled correlation $\tilde{\Phi}(r) = \Phi(r)/r^{-K_{sc}}$ for the models with $V = 0.2 \sim 1.0$ in folded Brillouin zone. (f) Intra-valley pairing of fermions within the same hole pocket.

where $\hat{\Delta}_\alpha^\dagger(x, y) = c_{(x, y)}^\dagger c_{(x, y) + \alpha}^\dagger$ is a pair creation operator on bond $\alpha = X, Y, Z$, as illustrated in Fig. 1(a). Here (x_0, y_0) is the reference bond taken as $x_0 \sim 5$ unit cells away from the open boundary and r is the distance between two bonds in the \mathbf{e}_1 direction. The colored bonds in Fig. 2(a) depict four different types of pair-pair correlations between bonds on same zigzag chain (Φ_{XX} , Φ_{ZZ}) and adjacent chains ($\Phi_{XX,1}$, $\Phi_{ZZ,1}$). At long distance, all four correlations exhibit sign-changing oscillations that alternate between negative (black) and positive (red) bonds. A direct comparison of correlations $\Phi_{XX}(r)$ and $\Phi_{XX,1}(r)$ is presented in Fig. 2(b), where r is the distance between two bonds along the \mathbf{e}_1 direction. Both correlation functions possess similar wavelength of ~ 3 unit cells and exhibit decaying behaviors that can be fitted by power-law functions. However, there is a roughly π -phase shift between the oscillations of $\Phi_{XX}(r)$ and $\Phi_{XX,1}(r)$. Combined these key features together, the pair correlation $\Phi(r)$ can be described generally as:

$$\Phi(r) \sim r^{-K_{sc}} \cos(Qr + \theta), \quad (3)$$

where Q is a non-zero ordering vector and K_{sc} is the power-law decay exponent. For $V = 1.0$, the extracted exponent $K_{sc} = 1.5(2)$ from Fig. 2(b), which suggests that the corresponding SC susceptibility $\chi_{sc} \sim T^{-(2-K_{sc})}$ diverges as the temperature $T \rightarrow 0$, under the assumption of emergent Lorentz symmetry in low energy

effective theories of 1+1D systems [81]. This establishes that the lightly doped spinless fermion model on six-leg cylinders has quasi-long-range SC correlations in the relatively strong V region.

Using the extracted exponent K_{sc} , we further define the scaled SC correlation function $\tilde{\Phi}(r) = \Phi(r)/r^{-K_{sc}}$ to investigate the spatial oscillation of the SC ordering. To determine the ordering vector Q in Eq. 3, we calculate the Fourier transform $\tilde{\Phi}(k) = \frac{1}{N} \sum_r e^{-ikr} \tilde{\Phi}(r)$ of the combination of $\tilde{\Phi}_{XX}(r)$ and $\tilde{\Phi}_{XX,1}(r)$ shown in Fig. 2(a) and (b). The ordering vector $Q \sim K = \{\frac{4\pi}{3\sqrt{3}}, 0\}$ is extracted from the pronounced peak of the orange line in Fig. 2(d). The pair momentum $Q \sim K$ can be explained by the intra-valley pairing of two fermions from the same hole pocket at $\pm K$ point. Note that the observed PDW is incommensurate as Q does not exactly match the $\pm K$ point. This deviation can arise from the asymmetric Fermi points illustrated in Fig. 2(f): the momentum of the Cooper pair is $k_1 + k_2 < 2K'$, which is equivalent to $k_1 + k_2 + 3K < 2K' + 3K = K$ as expected. It is intriguing that this incommensurate feature remains in the strong coupling region. Additionally, there are two subleading peaks around $\pm K/2$ points in $\tilde{\Phi}(k)$, which reflect the amplitude discrepancy between Φ_{XX} and $\Phi_{XX,1}$. The subleading peak can be removed by considering the Fourier transform of $\tilde{\Phi}_{XX}(r)$, where a single pair of prominent peaks corresponding to the

momentum Q appears in the folded Brillouin zone (BZ).

Once the leading ordering vector Q is determined, we investigate the evolution of the PDW ordering as V and L_x varied. We focus on the peaks of $\tilde{\Phi}_{XX}(k)$ in the folded BZ. The $\tilde{\Phi}_{XX}(k_x)$ of the systems with interaction $V = 0.2, 0.6, 1.0$ are summarized in Fig. 2(e). The single peak at $k = 0$ corresponds to the uniform BCS pairing which is dominant in the weak V region. When the interaction is gradually increased from $V = 0.2$ to $V = 1.0$, we observe that two peaks at finite-momentum $Q \sim \pm 2K$ emerge, and they become more dominant than the $k = 0$ one after the interaction exceeds a critical value $V_c \sim 0.6$, indicating the onset of the PDW state. The existence of PDW phase is further supported by the finite-size scaling of the peaks in the $V = 1.0$ model. As L_x increases, the finite-momentum peaks of $\tilde{\Phi}(k)$ become more pronounced, while the peak at zero momentum is suppressed (see SM for details), which suggests a dominating PDW order in the strong interaction regime.

We further investigate the potential PDW phase in systems with other V_2/V_1 and doping concentrations. Interestingly, our calculations show that for sufficiently large V_1 , the PDW phase could persist on the six-leg cylinder even when $V_2 = 0$. For instance, for the $V_2 = 0$ model on $L_x = 24$ cylinder with $\delta = 8.33\%$, a dominant peak of $\tilde{\Phi}(k)$ arises when V_1 is larger than ~ 1.0 (see SM for details). The momentum of the peaks does not obviously depend on the doping concentration, agreed with the picture of intra-valley pairing depicted in Fig. 2(f).

The charge density of the ground-state is $n(x, y) = \langle \hat{n}(x, y) \rangle$. For $V = 1.0$, $n(x, y)$ on the left part of the $L_x = 48$ cylinder is shown in Fig. 2(a). The density profile respects translation symmetry along \mathbf{e}_2 direction but has spatial oscillation with period $\lambda_c \sim 3$ along the \mathbf{e}_1 direction which decays quickly in the bulk. This spatial decay can be interpreted as the Friedel oscillation induced by the open boundary of the cylinder: $n(x) = A \cos(Q_c x + \phi) x^{-K_c/2} + \bar{n}$, where $Q_c = 2\pi/\lambda_c$ is the CDW ordering vector and K_c is the Luttinger exponent characterizing the density correlation [82]. We obtain $K_c \sim 1.7(3)$ which indicates a subdominant CDW correlation in the PDW phase (see SM for details).

PDW on wider systems: In many previous studies, evidences of PDW are observed mainly in models on 1D chains and narrow cylinders [59–61, 65–68]. Our study on six-leg cylinders is among the widest, but it is still essentially 1D in the sense that only the band with $k_y = 0$ crosses the 2D-limit Fermi surface. To have more bands crossing the 2D-limit Fermi surface, one needs to go to wider cylinders. So, we further studied the lightly doped model on eight-leg cylinders for which multiple bands (both $k_y = 0$ and $k_y \neq 0$) can cross the hole pocket Fermi surface, as shown in Fig. 1(b), such that it looks like a 2D FS. As a direct reflection of this dramatic change in low-energy physics, our DMRG simulation on the 8-leg model starts to observe non-trivial physical properties

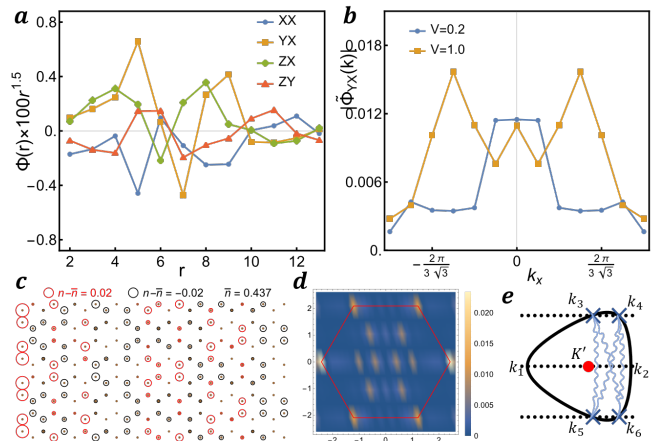


FIG. 3. PDW on 8-leg cylinders: (a) Scaled pair-pair correlation function $\tilde{\Phi}(r) = \Phi(r)/r^{-1.5}$ for the model with $V = 1.0$, $L_x = 21$, and doping $\delta \sim 12\%$. (b) Fourier transform of $\tilde{\Phi}(r)$ for the models with $V = 0.2$ and 1.0 . (c) Charge density profile of the model with $V = 1.0$. Radius of circles show the difference $n(x, y) - \bar{n}$ where \bar{n} is the average density, and black circle means negative value. (d) Fourier transform of the charge density profile in (c). (e) Examples of intra-valley pairing between multiple Fermi points for $L_y = 8$.

beyond 1D. For instance, from the density profile $n(x, y)$ of $V = 1.0$ and $\delta = 12\%$ model shown in Fig. 3(c), we can see that the translation symmetries along both \mathbf{e}_1 and \mathbf{e}_2 are broken, which is distinct from that of 6-leg cylinder. The Fourier transform of the charge density $n(\mathbf{k}) = \frac{1}{N} \sum e^{i\mathbf{k}\cdot\mathbf{r}} n(\mathbf{r})$ in Fig. 3(d) reveals details of additional symmetry breaking along \mathbf{e}_2 for 8-leg case: besides the two leading peaks at $\pm K$ points there are four additional sharp peaks appear at C_3 -rotation equivalent points of $\pm K$, indicating that the density profile tends to restore the C_6 rotation symmetry of the 2D lattice.

After observing the qualitative change in charge density profile for the wider system, one may naturally ask whether the PDW ordering persists when we extend the narrow cylinders to the 2D-like system. To answer this question, we investigate the possible PDW on 8-leg cylinders and positive evidences of robust PDW are obtained in our DMRG calculation of the 8-leg system. Due to the enormous amount of low-energy states introduced by multiple Fermi points, getting converged results on 8-leg cylinders is much more challenging computationally. To improve reliability of the DMRG results, we study cylinders with length up to $L_x = 21$ and push the bond dimension to $m = 33000$, which is state-of-the-art. Fig. 3(a) shows the long-distance behavior of the scaled pair-pair correlation function $\tilde{\Phi}(r) = \Phi(r)/r^{-1.5}$ for the $V = 1.0$ and $\delta = 12\%$ model on $L_x = 21$ cylinder, where we can clearly see the key feature of PDW ordering, i.e. the sign-changing oscillation, in all types of pair-pair correlation functions. After Fourier transform, the scaled correlation $\tilde{\Phi}(k)$ displays two finite-momentum peaks. Interestingly,

the location of these peaks provides insight into the underlying physics beyond 1D. As depicted in Fig. 3(f), the Cooper pair composed of fermions from 2D like FS can possess momentum larger than $2K'$, e.g. $k_3 + k_6 > 2K'$. Consequently, we observe in Fig. 3(b) that the peaks of $\tilde{\Phi}(k)$ have shifted from right side of $K/2$ (in six-leg case) to the left side. These peaks are replaced by a single peak at zero momentum in the $V = 0.2$ model, indicating that the emergence of PDW for $V = 1.0$ is a direct consequence of strong interactions.

Conclusion and discussions: We have studied the nature of SC in the lightly doped spinless fermion t - V_1 - V_2 model with finite Fermi surfaces and found robust signature of an incommensurate PDW state on 6-leg and 8-leg cylinders. On one hand, the pairing momentum close to $2K$ suggests that the intra-valley pairing plays an important role in forming the PDW state. On the other hand, the requirement of considerably strong interaction $V > V_c \sim 0.6$ to trigger the PDW order indicates that the PDW mechanism originates from strong coupling physics. It will be interesting to study in the future whether this mechanism is general, namely if it can appear in other systems featuring Dirac cones, such as the doped π -flux model on the square lattice and doped models of spinful fermions.

In the present model with doping $\delta \sim 12\%$, all the cylinders narrower than 8-leg are essentially 1D systems since their low-energy physics is characterized by the two Fermi points of a single band with $k_y = 0$. To the best of our knowledge, our study on the 8-leg cylinders with multiple bands crossing the Fermi level is probably the first one that shows robust evidence of an incommensurate PDW ordering in a model with 2D-like Fermi surface. As the t - V_1 - V_2 model on the honeycomb lattice may be potentially realized in systems such as twisted moire systems with spin polarization, e.g. Refs. [75–77], it could provide a promising arena to explore incommensurate PDW ground states in the future.

Acknowledgments: We would like to thank Steve Kivelson for helpful discussions. This work is supported in part by National Key R&D Program of China under Grant Nos. 2022YFA1402703 and 2021YFA1400100, the Innovation Program for Quantum Science and Technology under Grant No. 2021ZD0302502, Shanghai Pujiang Program under Grant No. 21PJ1410300, and the NSFC under Grant Nos. 12347107 and 12334003. H. Y. acknowledges the support in part by the Xplorer Prize through the New Cornerstone Science Foundation.

* jiangyf2@shanghaitech.edu.cn

† yaohong@tsinghua.edu.cn

- [1] J. Bardeen, L. N. Cooper, and J. R. Schrieffer, Theory of superconductivity, *Phys. Rev.* **108**, 1175 (1957).
 [2] A. I. Larkin and Y. N. Ovchinnikov, Inhomogeneous state

of superconductors, *Soviet Journal of Experimental and Theoretical Physics* **20**, 762 (1965).

- [3] P. Fulde and R. A. Ferrell, Superconductivity in a strong spin-exchange field, *Phys. Rev.* **135**, A550 (1964).
 [4] K. Gloos, R. Modler, H. Schimanski, C. D. Bredl, C. Geibel, F. Steglich, A. I. Buzdin, N. Sato, and T. Komatsubara, Possible formation of a nonuniform superconducting state in the heavy-fermion compound UPd_2Al_3 , *Phys. Rev. Lett.* **70**, 501 (1993).
 [5] R. Modler, P. Gegenwart, M. Lang, M. Deppe, M. Weiden, T. Lühmann, C. Geibel, F. Steglich, C. Paulsen, J. L. Tholence, N. Sato, T. Komatsubara, Y. Ōnuki, M. Tachiki, and S. Takahashi, First-order transition between weak and strong pinning in clean superconductors with enhanced spin susceptibility, *Phys. Rev. Lett.* **76**, 1292 (1996).
 [6] A. Yamashita, K. Ishii, T. Yokoo, J. Akimitsu, M. Hedo, Y. Inada, Y. Ōnuki, E. Yamamoto, Y. Haga, and R. Kadono, Anomalous field dependence of magnetic penetration depth in the vortex state of CeRu_2 probed by muon spin rotation, *Phys. Rev. Lett.* **79**, 3771 (1997).
 [7] H. A. Radovan, N. A. Fortune, T. P. Murphy, S. T. Hannahs, E. C. Palm, S. W. Tozer, and D. Hall, Magnetic enhancement of superconductivity from electron spin domains, *Nature* **425**, 51 (2003).
 [8] A. Bianchi, R. Movshovich, C. Capan, P. G. Pagliuso, and J. L. Sarrao, Possible Fulde-Ferrell-Larkin-Ovchinnikov superconducting state in CeCoIn_5 , *Phys. Rev. Lett.* **91**, 187004 (2003).
 [9] C.-w. Cho, J. H. Yang, N. F. Q. Yuan, J. Shen, T. Wolf, and R. Lortz, Thermodynamic evidence for the Fulde-Ferrell-Larkin-Ovchinnikov state in the KFe_2As_2 superconductor, *Phys. Rev. Lett.* **119**, 217002 (2017).
 [10] C. C. Agosta, Inhomogeneous superconductivity in organic and related superconductors, *Crystals* **8**, 285 (2018).
 [11] S. Kasahara, Y. Sato, S. Licciardello, M. Čulo, S. Arsenijević, T. Ottenbros, T. Tominaga, J. Böker, I. Eremin, T. Shibauchi, J. Wosnitza, N. E. Hussey, and Y. Matsuda, Evidence for an Fulde-Ferrell-Larkin-Ovchinnikov state with segmented vortices in the BCS-BEC-Crossover superconductor FeSe , *Phys. Rev. Lett.* **124**, 107001 (2020).
 [12] D. F. Agterberg, J. C. S. Davis, S. D. Edkins, E. Fradkin, D. J. Van Harlingen, S. A. Kivelson, P. A. Lee, L. Radzihovsky, J. M. Tranquada, and Y. X. Wang, The physics of pair-density waves: Cuprate superconductors and beyond, *Annu. Rev. Condens. Matter Phys.* **11**, 231 (2020).
 [13] Q. Li, M. Hücker, G. D. Gu, A. M. Tsvelik, and J. M. Tranquada, Two-dimensional superconducting fluctuations in stripe-ordered $\text{La}_{1.875}\text{Ba}_{0.125}\text{CuO}_4$, *Phys. Rev. Lett.* **99**, 067001 (2007).
 [14] E. Berg, E. Fradkin, E. A. Kim, S. A. Kivelson, V. Oganesyan, J. M. Tranquada, and S. C. Zhang, Dynamical layer decoupling in a stripe-ordered high-Tc superconductor, *Phys. Rev. Lett.* **99**, 127003 (2007).
 [15] D. F. Agterberg and H. Tsunetsugu, Dislocations and vortices in pair-density-wave superconductors, *Nature Physics* **4**, 639 (2008).
 [16] E. Berg, E. Fradkin, and S. A. Kivelson, Charge-4e superconductivity from pair-density-wave order in certain high-temperature superconductors, *Nature Physics* **5**, 830 (2009).
 [17] E. Fradkin, S. A. Kivelson, and J. M. Tranquada, Collo-

- quium: Theory of intertwined orders in high temperature superconductors, *Rev. Mod. Phys.* **87**, 457 (2015).
- [18] M. H. Hamidian, S. D. Edkins, S. H. Joo, A. Kostin, H. Eisaki, S. Uchida, M. J. Lawler, E. A. Kim, A. P. Mackenzie, K. Fujita, J. Lee, and J. C. Davis, Detection of a Cooper-pair density wave in $\text{Bi}_2\text{Sr}_2\text{CaCu}_2\text{O}_{8+x}$, *Nature* **532**, 343 (2016).
- [19] W. Ruan, X. T. Li, C. Hu, Z. Q. Hao, H. W. Li, P. Cai, X. J. Zhou, D. H. Lee, and Y. Y. Wang, Visualization of the periodic modulation of Cooper pairing in a cuprate superconductor, *Nature Physics* **14**, 1178 (2018).
- [20] S. D. Edkins, A. Kostin, K. Fujita, A. P. Mackenzie, H. Eisaki, S. Uchida, S. Sachdev, M. J. Lawler, E.-A. Kim, J. C. Séamus Davis, and M. H. Hamidian, Magnetic field induced pair density wave state in the cuprate vortex halo, *Science* **364**, 976 (2019).
- [21] Z. Du, H. Li, S. H. Joo, E. P. Donoway, J. Lee, J. C. S. Davis, G. Gu, P. D. Johnson, and K. Fujita, Imaging the energy gap modulations of the cuprate pair-density-wave state, *Nature* **580**, 65 (2020).
- [22] X. Li, C. Zou, Y. Ding, H. Yan, S. Ye, H. Li, Z. Hao, L. Zhao, X. Zhou, and Y. Wang, Evolution of charge and pair density modulations in overdoped $\text{Bi}_2\text{Sr}_2\text{CuO}_{6+\delta}$, *Phys. Rev. X* **11**, 011007 (2021).
- [23] H. Zhao, R. Blackwell, M. Thinel, T. Handa, S. Ishida, X. Zhu, A. Iyo, H. Eisaki, A. N. Pasupathy, and K. Fujita, Smectic pair-density-wave order in $\text{EuRbFe}_4\text{As}_4$, *Nature* **618**, 940 (2023).
- [24] Y. Liu, T. Wei, G. He, Y. Zhang, Z. Wang, and J. Wang, Pair density wave state in a monolayer high- T_c iron-based superconductor, *Nature* **618**, 934 (2023).
- [25] Q. Gu, J. P. Carroll, S. Wang, S. Ran, C. Broyles, H. Siddiquee, N. P. Butch, S. R. Saha, J. Paglione, J. C. S. Davis, and X. Liu, Detection of a pair density wave state in UTe_2 , *Nature* **618**, 921 (2023).
- [26] A. Aishwarya, J. May-Mann, A. Raghavan, L. Nie, M. Romanelli, S. Ran, S. R. Saha, J. Paglione, N. P. Butch, E. Fradkin, and V. Madhavan, Magnetic-field-sensitive charge density waves in the superconductor UTe_2 , *Nature* **618**, 928 (2023).
- [27] H. Chen, H. Yang, B. Hu, Z. Zhao, J. Yuan, Y. Xing, G. Qian, Z. Huang, G. Li, Y. Ye, S. Ma, S. Ni, H. Zhang, Q. Yin, C. Gong, Z. Tu, H. Lei, H. Tan, S. Zhou, C. Shen, X. Dong, B. Yan, Z. Wang, and H.-J. Gao, Roton pair density wave in a strong-coupling kagome superconductor, *Nature* **599**, 222 (2021).
- [28] A. Himeda, T. Kato, and M. Ogata, Stripe states with spatially oscillating d -wave superconductivity in the two-dimensional $t-t'-J$ model, *Phys. Rev. Lett.* **88**, 117001 (2002).
- [29] M. Raczkowski, M. Capello, D. Poilblanc, R. Frésard, and A. M. Oleś, Unidirectional d -wave superconducting domains in the two-dimensional $t-J$ model, *Phys. Rev. B* **76**, 140505 (2007).
- [30] C. Wu, K. Sun, E. Fradkin, and S.-C. Zhang, Fermi liquid instabilities in the spin channel, *Phys. Rev. B* **75**, 115103 (2007).
- [31] A. Aperis, G. Varelogiannis, P. B. Littlewood, and B. D. Simons, Coexistence of spin density wave, d -wave singlet and staggered π -triplet superconductivity, *J. Phys.: Condens. Matter* **20**, 434235 (2008).
- [32] K.-Y. Yang, W. Q. Chen, T. M. Rice, M. Sigrist, and F.-C. Zhang, Nature of stripes in the generalized t - J model applied to the cuprate superconductors, *New Journal of Physics* **11**, 055053 (2009).
- [33] B. Roy and I. F. Herbut, Unconventional superconductivity on honeycomb lattice: Theory of kekule order parameter, *Phys. Rev. B* **82**, 035429 (2010).
- [34] F. Loder, S. Graser, A. P. Kampf, and T. Kopp, Mean-field pairing theory for the charge-stripe phase of high-temperature cuprate superconductors, *Phys. Rev. Lett.* **107**, 187001 (2011).
- [35] Y.-Z. You, Z. Chen, X.-Q. Sun, and H. Zhai, Superfluidity of bosons in kagome lattices with frustration, *Phys. Rev. Lett.* **109**, 265302 (2012).
- [36] G. Y. Cho, J. H. Bardarson, Y.-M. Lu, and J. E. Moore, Superconductivity of doped Weyl semimetals: Finite-momentum pairing and electronic analog of the ^3He - A phase, *Phys. Rev. B* **86**, 214514 (2012).
- [37] P. A. Lee, Amperean pairing and the pseudogap phase of cuprate superconductors, *Phys. Rev. X* **4**, 031017 (2014).
- [38] R. Soto-Garrido and E. Fradkin, Pair-density-wave superconducting states and electronic liquid-crystal phases, *Phys. Rev. B* **89**, 165126 (2014).
- [39] R. Soto-Garrido, G. Y. Cho, and E. Fradkin, Quasi-one-dimensional pair density wave superconducting state, *Phys. Rev. B* **91**, 195102 (2015).
- [40] S. K. Jian, Y. F. Jiang, and H. Yao, Emergent space-time supersymmetry in 3D weyl semimetals and 2D dirac semimetals, *Phys. Rev. Lett.* **114**, 237001 (2015).
- [41] Y. Wang, D. F. Agterberg, and A. Chubukov, Coexistence of charge-density-wave and pair-density-wave orders in underdoped cuprates, *Phys. Rev. Lett.* **114**, 197001 (2015).
- [42] J. Wårdh and M. Granath, Effective model for a supercurrent in a pair-density wave, *Phys. Rev. B* **96**, 224503 (2017).
- [43] J. Wårdh, B. M. Andersen, and M. Granath, Suppression of superfluid stiffness near a Lifshitz-point instability to finite-momentum superconductivity, *Phys. Rev. B* **98**, 224501 (2018).
- [44] Z. Han, S. A. Kivelson, and H. Yao, Strong coupling limit of the Holstein-Hubbard model, *Phys. Rev. Lett.* **125**, 167001 (2020).
- [45] T. Li, J. Ingham, and H. D. Scammell, Artificial graphene: Unconventional superconductivity in a honeycomb superlattice, *Phys. Rev. Res.* **2**, 043155 (2020).
- [46] D. Chakraborty and A. M. Black-Schaffer, Odd-frequency pair density wave correlations in underdoped cuprates, *New Journal of Physics* **23**, 033001 (2021).
- [47] C. Setty, J. Zhao, L. Fanfarillo, E. W. Huang, P. J. Hirschfeld, P. W. Phillips, and K. Yang, Exact solution for finite center-of-mass momentum Cooper pairing (2022), [arXiv:2209.10568 \[cond-mat.supr-con\]](https://arxiv.org/abs/2209.10568).
- [48] J.-T. Jin, K. Jiang, H. Yao, and Y. Zhou, Interplay between pair density wave and a nested fermi surface, *Phys. Rev. Lett.* **129**, 167001 (2022).
- [49] Z. Han and S. A. Kivelson, Pair density wave and reentrant superconducting tendencies originating from valley polarization, *Phys. Rev. B* **105**, L100509 (2022).
- [50] P. Coleman, A. Panigrahi, and A. Tsvelik, Solvable 3D kondo lattice exhibiting pair density wave, odd-frequency pairing, and order fractionalization, *Phys. Rev. Lett.* **129**, 177601 (2022).
- [51] T. Li, M. Geier, J. Ingham, and H. D. Scammell, Higher-order topological superconductivity from repulsive interactions in kagome and honeycomb systems, *2D Materials*

- 9**, 015031 (2021).
- [52] D. Shaffer, F. J. Burnell, and R. M. Fernandes, Weak-coupling theory of pair density wave instabilities in transition metal dichalcogenides, *Phys. Rev. B* **107**, 224516 (2023).
- [53] D. Shaffer and L. H. Santos, Triplet pair density wave superconductivity on the π -flux square lattice, *Phys. Rev. B* **108**, 035135 (2023).
- [54] Y.-M. Wu, P. A. Nosov, A. A. Patel, and S. Raghu, Pair density wave order from electron repulsion, *Phys. Rev. Lett.* **130**, 026001 (2023).
- [55] Y.-M. Wu, Z. Wu, and H. Yao, Pair-density-wave and chiral superconductivity in twisted bilayer transition metal dichalcogenides, *Phys. Rev. Lett.* **130**, 126001 (2023).
- [56] G. Jiang and Y. Barlas, Pair density waves from local band geometry, *Phys. Rev. Lett.* **131**, 016002 (2023).
- [57] C. Setty, L. Fanfarillo, and P. J. Hirschfeld, Mechanism for fluctuating pair density wave, *Nature Communications* **14**, 3181 (2023).
- [58] T. Schwemmer, H. Hohmann, M. Dürrnagel, J. Potten, J. Beyer, S. Rachel, Y.-M. Wu, S. Raghu, T. Müller, W. Hanke, *et al.*, Pair density wave instability in the kagome Hubbard model, arXiv preprint arXiv:2302.08517 (2023).
- [59] E. Berg, E. Fradkin, and S. A. Kivelson, Pair-density-wave correlations in the Kondo-Heisenberg model, *Phys. Rev. Lett.* **105**, 146403 (2010).
- [60] A. Jaefari and E. Fradkin, Pair-density-wave superconducting order in two-leg ladders, *Phys. Rev. B* **85**, 035104 (2012).
- [61] J. Venderley and E. A. Kim, Evidence of pair-density wave in spin-valley locked systems, *Sci. Adv.* **5**, eaat4698 (2019).
- [62] Y.-H. Zhang and A. Vishwanath, Pair-density-wave superconductor from doping Haldane chain and rung-singlet ladder, *Phys. Rev. B* **106**, 045103 (2022).
- [63] S. Zhou and Z. Wang, Chern fermi pocket, topological pair density wave, and charge-4e and charge-6e superconductivity in kagomé superconductors, *Nature Communications* **13**, 7288 (2022).
- [64] F. Chen and D. Sheng, Singlet, triplet and pair density wave superconductivity in the doped triangular-lattice moiré system, arXiv preprint arXiv:2302.06765 (2023).
- [65] H.-C. Jiang, Pair density wave in the doped three-band Hubbard model on two-leg square cylinders, *Phys. Rev. B* **107**, 214504 (2023).
- [66] X. Y. Xu, K. T. Law, and P. A. Lee, Pair density wave in the doped t-J model with ring exchange on a triangular lattice, *Phys. Rev. Lett.* **122**, 167001 (2019).
- [67] C. Peng, Y. F. Jiang, T. P. Devereaux, and H. C. Jiang, Precursor of pair-density wave in doping Kitaev spin liquid on the honeycomb lattice, *Npj Quantum Materials* **6**, 64 (2021).
- [68] C. Peng, Y.-F. Jiang, Y. Wang, and H.-C. Jiang, Gapless spin liquid and pair density wave of the Hubbard model on three-leg triangular cylinders, *New Journal of Physics* **23**, 123004 (2021).
- [69] K. S. Huang, Z. Han, S. A. Kivelson, and H. Yao, Pair-density-wave in the strong coupling limit of the Holstein-Hubbard model, *npj Quantum Materials* **7**, 17 (2022).
- [70] S. R. White, Density matrix formulation for quantum renormalization groups, *Phys. Rev. Lett.* **69**, 2863 (1992).
- [71] S. Capponi and A. M. Läuchli, Phase diagram of interacting spinless fermions on the honeycomb lattice: A comprehensive exact diagonalization study, *Phys. Rev. B* **92**, 085146 (2015).
- [72] S. Capponi, Phase diagram of interacting spinless fermions on the honeycomb lattice, *J. Phys.: Condens. Matter.* **29**, 043002 (2017).
- [73] Y. Cao, V. Fatemi, S. Fang, K. Watanabe, T. Taniguchi, E. Kaxiras, and P. Jarillo-Herrero, Unconventional superconductivity in magic-angle graphene superlattices, *Nature* **556**, 43 (2018).
- [74] Y. Cao, V. Fatemi, A. Demir, S. Fang, S. L. Tomarken, J. Y. Luo, J. D. Sanchez-Yamagishi, K. Watanabe, T. Taniguchi, E. Kaxiras, R. C. Ashoori, and P. Jarillo-Herrero, Correlated insulator behaviour at half-filling in magic-angle graphene superlattices, *Nature* **556**, 80 (2018).
- [75] X. Liu, Z. Hao, E. Khalaf, J. Y. Lee, Y. Ronen, H. Yoo, D. Haei Najafabadi, K. Watanabe, T. Taniguchi, A. Vishwanath, and P. Kim, Tunable spin-polarized correlated states in twisted double bilayer graphene, *Nature* **583**, 221 (2020).
- [76] K. Slagle and L. Fu, Charge transfer excitations, pair density waves, and superconductivity in moiré materials, *Phys. Rev. B* **102**, 235423 (2020).
- [77] T. Devakul, V. Crépel, Y. Zhang, and L. Fu, Magic in twisted transition metal dichalcogenide bilayers, *Nature Communications* **12**, 6730 (2021).
- [78] G. B. Partridge, W. Li, R. I. Kamar, Y. an Liao, and R. G. Hulet, Pairing and phase separation in a polarized fermi gas, *Science* **311**, 503 (2006), <https://www.science.org/doi/pdf/10.1126/science.1122876>.
- [79] G. Jotzu, M. Messer, R. Desbuquois, M. Lebrat, T. Uehlinger, D. Greif, and T. Esslinger, Experimental realization of the topological haldane model with ultracold fermions, *Nature* **515**, 237 (2014).
- [80] H.-S. Kim and H.-Y. Kee, Realizing haldane model in fe-based honeycomb ferromagnetic insulators, *npj Quantum Materials* **2**, 20 (2017).
- [81] E. Arrighoni, E. Fradkin, and S. A. Kivelson, Mechanism of high-temperature superconductivity in a striped hubbard model, *Phys. Rev. B* **69**, 214519 (2004).
- [82] S. R. White, I. Affleck, and D. J. Scalapino, Friedel oscillations and charge density waves in chains and ladders, *Phys. Rev. B* **65**, 1651221 (2002).

SUPPLEMENTAL MATERIAL

A. Numerical Details

In the present work, we performed the GPU-accelerated DMRG simulations with charge U(1) symmetry to study the ground-state properties of the t - V_1 - V_2 model. The matrix multiplication heavily used in Lanczos algorithms for solving ground-state of the effective Hamiltonian and the truncation of the Hilbert space can be greatly accelerated by GPU processors. To obtain reliable pair-pair correlation functions on wide cylinders, we performed an extrapolation for correlation functions to the zero truncation-error limit $\epsilon \rightarrow 0$ (i.e. $m \rightarrow \infty$). For example, on $L_x = 15$ and $L_y = 8$ cylinder, we first calculate correlation $\Phi_{ZZ}(\epsilon)$ by keeping $m = 22000 \sim 33000$ states for each r . For each number of states m , we performed at least 5 DMRG sweeps to reach converged results. Then, an extrapolation using a second-order polynomial $\Phi_{ZZ}(\epsilon) = \Phi_{ZZ} + a_1\epsilon + a_2\epsilon^2$ is applied to extract Φ_{ZZ} to the zero truncation-error limit for each r . Here ϵ is the truncation-error associated with the number of states m , and a_1 and a_2 are fitting parameters. As shown by the dense data points in Fig. S1(a), the fitting qualities are quite good even for long-distance correlations. We further present the finite-truncation error extrapolation for correlation functions $\Phi_{YX}(r)$ and $\Phi_{ZY}(r)$ on the $L_x = 21$ and $L_y = 8$ cylinder in Fig. S1(b) and (c), respectively.

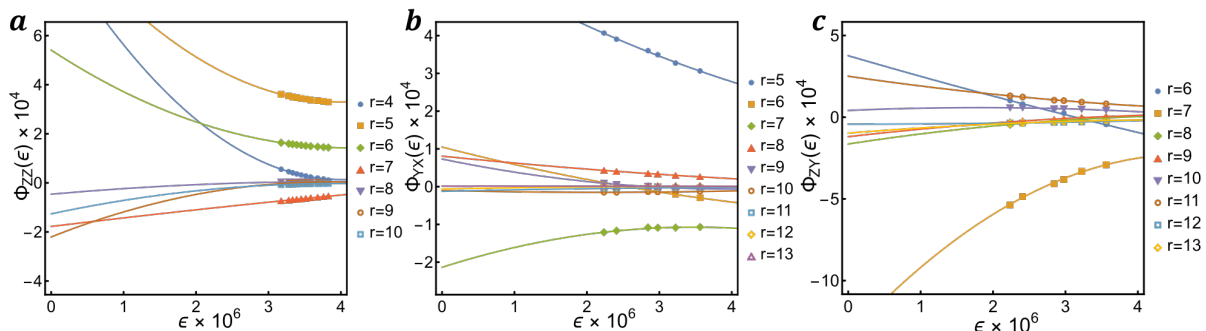


FIG. S1. Finite-truncation-error extrapolation for pair-pair correlation measured on 8-leg cylinders with $m = 22,000 \sim 33,000$ DMRG block states. (a) The correlation $\Phi_{ZZ}(r, \epsilon)$ as a function of truncation ϵ obtained on $L_x = 15$ and $L_y = 8$ cylinders, r is the distance between two bonds along the zigzag chain. (b) The correlation $\Phi_{YX}(r, \epsilon)$ on $L_x = 21$ and $L_y = 8$ cylinders. (c) The correlation $\Phi_{ZY}(r, \epsilon)$ on $L_x = 21$ and $L_y = 8$ cylinders.

B. Evidences of PDW for the case of $V_2/V_1 = 0$, for other cases of V_2/V_1 , and for different doping δ

Here we provide further numerical evidences of the PDW phase across a range of V_2/V_1 ratios and doping concentrations δ . We choose various values of V_2/V_1 between 0 and $2/3$, and perform the simulations on the $2 \times 24 \times 6$ systems with doping $\delta = 1/12$ and $1/9$. One important observation is that the PDW order can be solely induced with a strong V_1 attraction. As shown in Fig. S2(a), for $\delta = 1/12$ and $V_2 = 0$, the Fourier transform of the scaled correlation function $\tilde{\Phi}_{XX}(k)$ exhibits dominant finite momentum peaks when V_1 exceeds a relatively larger threshold 1.0, indicating the key role of the V_1 interaction in inducing PDW ordering. Here the same exponent $K_{sc} = 1.5$ is used for all three correlation functions to ensure consistency. Similar to the finite V_2 case discussed in the main text, the location of the peak indicates the momentum of the Cooper pairs is around $2K$. The small deviation between the location of peak and $2K$ is smeared out by the relatively large interval of k_x caused the small system size.

We also consider other V_2/V_1 ratios and doping δ as summarized in Fig. S2(b). For $\delta = 1/9$, the PDW ordering for finite V_1 but $V_2 = 0$ is also observed, which clearly suggest that PDW can exist in a finite range of doping concentration around 10%. The effect of V_2 in forming the PDW state is complex. A weak V_2 is helpful to form PDW since it reduce the critical V_1 required for establishing the PDW order. However, there is an optimal ratio V_2/V_1 for PDW; when the ratio is too large, it can suppress PDW. For instance, when V_2 becomes comparable to V_1 , e.g. $V_2/V_1 = \frac{2}{3}$, the spatial oscillation of the pair-pair correlation is suppressed.

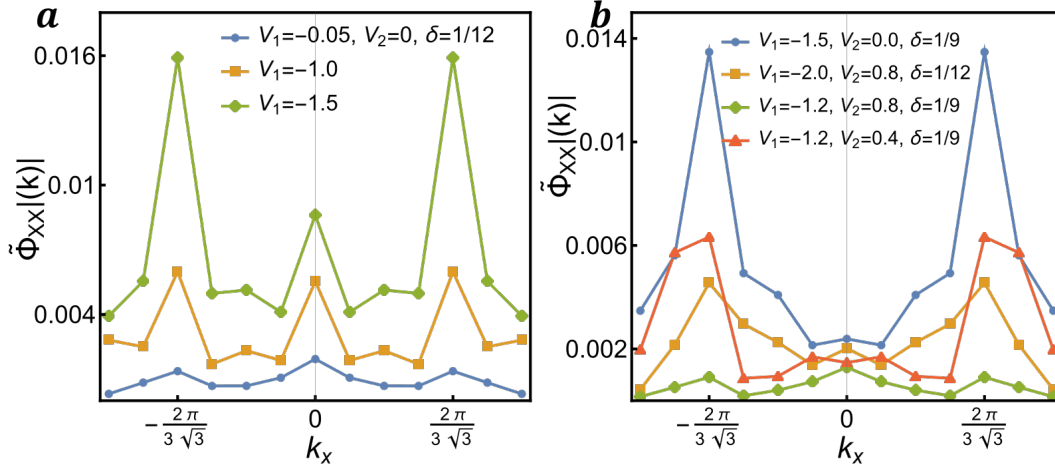


FIG. S2. Fourier transform of scaled correlation function for a series of V_2/V_1 ratios and doping δ . The same exponent $K = 1.5$ is used to scale the correlation $\Phi(r)$ for all the cases.

C. PDW peaks in systems with different length

To rule out possible finite size effect, we further calculate $\tilde{\Phi}(k)$ of the $V = 0.2$ and 1.0 models on the cylinder with $L_x = 24 \sim 48$, as depicted in Fig. S3. Again, we fix $V_1 = -V$ and $V_2 = V/2$, and apply same uniform scaling factor $K = 1.5$ to normalize the correlation functions. For the weakly interacting model with $V = 0.2$ and $\delta = 11.1\%$, we find that the finite-momentum peaks are suppressed as the length increases from $L_x = 36$ to 48 ; on the contrary, the zero-momentum peak gradually increases and becomes dominant in the $L_x = 48$ system. This result implies that at weak coupling the uniform SC is preferred in the ground state, as expected. The opposite behavior happens for the strong interaction case of $V = 1.0$, as shown in Fig. S3(b); as L_x increases, the finite-momentum peaks of $\tilde{\Phi}(k)$ become sharper while the zero-momentum peak is suppressed, which clearly suggests that for strong interaction $V = 1.0$ the PDW with finite-momentum pairing is the only dominant SC order.

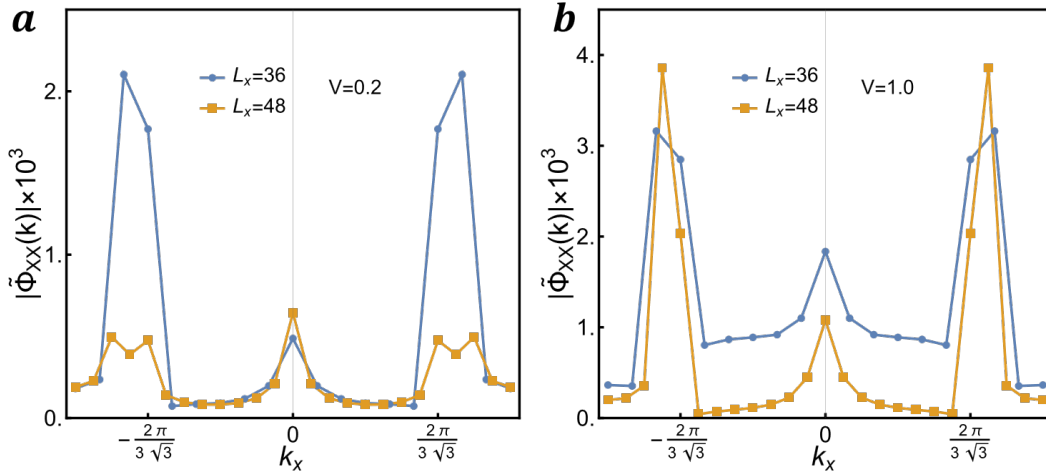


FIG. S3. Fourier transform of scaled correlation function for the $V = 0.2$ and $V = 1.0$ models on $L_x = 36, 48$ cylinders with doping $\delta = 11.1\%$. The same exponent $K = 1.5$ is used to rescale the correlation $\Phi(r)$ for all three systems.

D. Quasi-long-range CDW on six-leg cylinder

Here we show more results about charge density properties on the six-leg cylinder. The density profile $\langle n(x, y) \rangle$ obtained on the longest cylinder with $L_x = 48$ is shown in Fig. S4(a), where we can find the density wave has spatial

decaying in the bulk. The doping concentration is $\delta = 11.1\%$ and interaction $V = 1.0$. To precisely determine the long-distance behavior, we calculate the rung average of the density profile $\langle n(x) \rangle = \frac{1}{L_y} \sum_y \langle n(x, y) \rangle$. As shown in Fig. S4(b), the spatial decaying of the rung density $\langle n(x) \rangle$ is accompanied with a complicated oscillation caused by the two-site unit cell. We further average the electron density on two sub-lattice in each unit-cell $\tilde{n}(\tilde{x}) = (n_A(\tilde{x}) + n_B(\tilde{x}))/2$, where \tilde{x} labels the unit cell counted from the open boundary of the cylinder. The average density $\tilde{n}(\tilde{x})$ can be accurately fitted by the Friedel oscillation

$$\tilde{n}(\tilde{x}) = A \cos(Q_c \tilde{x} + \phi) \tilde{x}^{-K_c/2} + \bar{n}, \quad (\text{S1})$$

where Q_c is the ordering momentum of CDW and K_c is the Luttinger exponent characterizing the long-distance behaviors of density-density correlation function. As shown in Fig. S4(c), the exponent extracted from Friedel oscillation is $K_c = 1.7(3)$ and the ordering momentum Q_c is around $2\pi/3.5$, i.e. the wavelength of the CDW is ~ 3.5 unit cells. Note the exponent of SC correlation function obtained on the same system is $K_{sc} \sim 1.5 < K_c$, implying that the PDW ordering is the most dominant order.

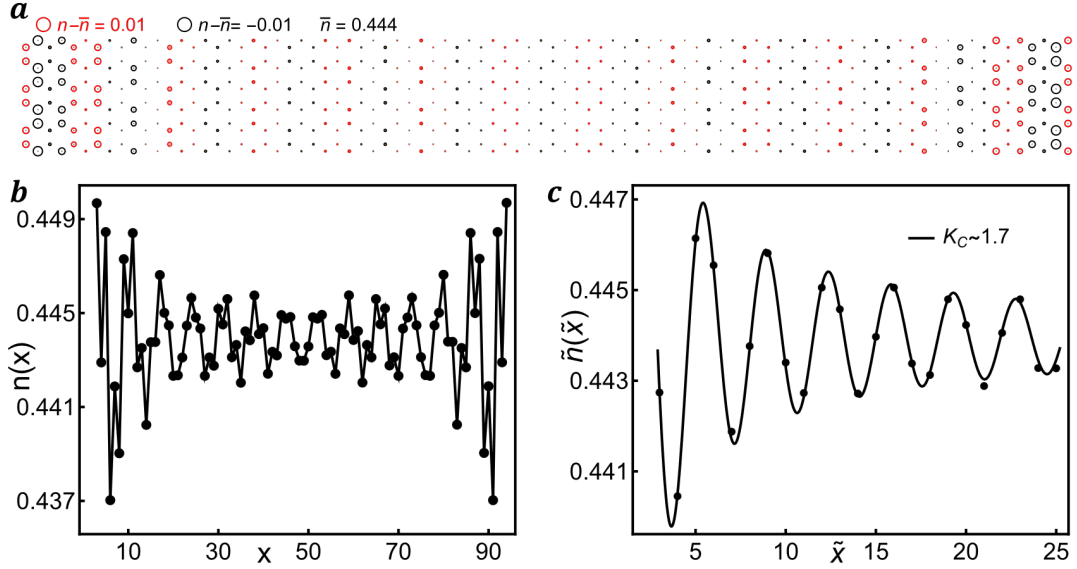


FIG. S4. The density properties of the $V = 1.0$ model on the six-leg cylinders with $L_x = 48$ and $\delta = 11.1\%$: (a) the density profile of the system. Two unit cells at boundaries are omitted. (b) The rung density $n(x)$ of the system, where x labels the site. (c) The average density of the unit cell $\tilde{n}(\tilde{x})$, where \tilde{x} labels the unit cell. Solid line represents the fitting result of the Friedel oscillation.